Prediction of Aeroelastic Flutter in a Hard Disk Drive

Byoung-Cheol Kim, Arvind Raman
Dynamic Stability Laboratory
1113 Etcheverry Hall
University of California
Berkeley, CA94720
e-mail:bckim@mote.me.berkeley.edu
e-mail:arvind@mote.me.berkeley.edu

C. D. Mote, Jr.
Glenn L. Martin Institute
Professor of Engineering and President
University of Maryland
College Park, MD20742
e-mail: dmote@deans.umd.edu

Abstract

An experimental technique to predict the onset of aeroelastic flutter of an enclosed computer memory disk is presented. The aerodynamic force is modeled by the sum of dissipative and circulatory linear operators which subsumes as a special case the pressure generated in a thin hydrodynamic film between the disk and the wall. It is shown that the aeroelastic model parameters can be extracted from the Frequency Response Function of the disk spinning at subcritical speeds. The aeroelastic parameters for an acoustically excited single disk at different enclosure gaps are derived for the speed range 6,000-19,800 rpm. The flutter speed predicted is strongly influenced by the enclosure gap and the substrate damping. Flutter speed as low as 35,000 rpm has been predicted. The technique can also be extended to predict the flutter speeds in other systems including DVD and CDROM drives.

1 Introduction

The new generation of hard disk drives is expected to pack very high track densities (20, 000 + tpi) and rotate at very high speeds (20, 000 + rpm). At rotation speeds near and beyond 20, 000 rpm the aeroelastic coupling between the disk vibration and the air around disk is expected to be significant. This coupling leads to disk flutter which would contribute significantly to track misregistration and disk drive failure. Thus, the prediction of the aeroelastic flutter speed is crucial for the design of the new generation of disk drives.

The stability of the equilibrium configuration of floppy disks coupled through thin gas films to a rigid enclosure have been studied by a number of researchers (Chonan *et al*. (1992), Hosaka and Crandall (1992), Huang and Mote (1995), Huang and Mote (1996), Renshaw (1998)). While Chonan *et al*. (1992) modeled the film as a linear elastic foundation, Hosaka and Crandall (1992) and Renshaw (1998) utilized thin film lubrication equations neglecting the effect of radial flow. Huang and Mote (1996) included the effect of radial flow and concluded that non-symmetric stiffening caused by the radial flow can cause combination instabilities in addition to aeroelastic flutter. These have hitherto been theoretical and numerical studies only.

Aeroelastic coupling problems in a hard disk, however, are distinct from those for a floppy disk for the following reasons:

1. Rotation speeds in hard disk drives are greater than in floppy disks, and the gap widths are greater. This leads to substantially greater flow Reynolds number and the use of hydrodynamic lubrication theory can lead to an inaccurate model of the aerodynamic pressure. The Reynolds number, for a commercially available 3.5 inch hard disk rotating at 10,000 rpm (Ω : disk speed, R_2: outer disk radius, d : gap spacing between the disk and the wall) is substantially greater than 1 ($R_e = \frac{\Omega R_2 d}{n} = 663 >> 1$). Note that Reynolds number of the flow between two corotating disks in a disk stack will be greater than this value because inter-disk spacing is usually greater than spacing between disk and wall.

2. Hard disks have high bending stiffness and for satisfactory operations the disk must maintain a near flat equilibrium.
3. The aluminum substrate in the disk has high significant material damping which must be modeled.
4. Multiple disk stacks are normal and the outer disks in a stack are subject to dissimilar flow conditions on their faces. A shear flow between the disk and rigid enclosure exists on one surface and flow in a corotating enclosure is present on the other side. Are outer disks more susceptible to flutter than the inner ones?

This work presents an experimental estimation technique for the flutter speed of a hard disk based on measurements taken at subcritical speeds. The technique is based on a simple fluid pressure model represented by a distributed, viscous pressure that rotates with respect to the disk, in a manner analogous to Hansen *et al.* (1998). This model approaches to the special case of the pressure generated in a narrow gap at low Reynolds number. It is shown analytically that this form of aerodynamic loading differentially damps the forward and backward traveling waves. To illustrate this point, the frequency response function of an aerodynamically excited disk spinning at 19,800 rpm is shown in Fig. 1. The peaks represent travelling wave frequencies and the modes are labeled as shown. It is seen that the forward travelling waves are more highly damped than the backward travelling waves. For instance, the forward travelling wave peak magnitude for the (0,2) mode is nearly 17 dB lower than backward travelling wave peak magnitude. The 3 dB bandwidth for forward travelling wave ($\approx$ 10 dB) is much greater than backward travelling wave ($\approx$ 4 dB). This differential damping is primarily due to air flow effects because in vacuum the damping of forward and backward travelling waves is identical (Hansen *et al.* (1998)). At higher speeds damping of the backward travelling waves can vanish entirely leading to travelling wave flutter instability. This result is exploited to extract model parameters from the Frequency Response Function (FRF) of the acoustically excited disk at subcritical speeds. The method of Hansen *et al.* (1998) is used to predict the supercritical speed at which the damping of a backward traveling wave vanishes and aeroelastic flutter occurs.

The results show that the flutter speed and mode are strongly dependent on the enclosure gap width. The flutter speed can be as low as 35,000 rpm. Strong dependence of the flutter speed on the gap width confirms that the onset of flutter can be affected

through airflow control through enclosure design. The results also indicate that the onset of the aeroelastic flutter should not be a concern for the impending generation of 20,000 rpm drives, but possibly for the next generation of 30,000 + rpm drives. Lastly, the technique used here can be applied to predict the flutter speeds of optical disk systems used in CDROM and DVD drives. Because the bending stiffness and natural frequencies are much smaller in these polycarbonate substrate disks, their flutter speeds will also be lower. We note that CDROM drives have recently been shown to operate at supercritical speeds (Lee *et al.* (1998)) and thus operate much closer to their aeroelastic flutter speeds.

2 Theoretical background

The theoretical development here is based on the work of Hansen *et al.* (1998). Consider a single annular disk of thickness h, clamping radius a, and outer radius b. Each disk can be modeled as isolated if the effects of spindle flexibility and bearing clearance are neglected. The disk substrate is assumed to be isotropic, with Young's Modulus E, Poisson's ratio n, and density r. Thedisk spins at a constant speed Ω^*. A ground-fixed cylindrical coordinate frame (r^*, j, z^*) is introduced. Acoustic waves from a speaker, over a small circular area centered around point (r_f^*, j_f), are used to excite the disk transversely. The aerodynamic pressure difference across the two faces of the disk is Δp^*. Because of the large bending stiffness the disk remains flat at equilibrium in the presence of aerodynamic pressure gradients. The governing equations for small amplitude transverse oscillations, $w(r^*, j, t^*)$, of a flat, spinning, linearly elastic disk have been presented by several authors (Hosaka and Crandall (1992), Renshaw (1998), Hansen *et al* (1998)). With inclusion of the aerodynamic loading and acoustic excitation and the introduction of the dimensionless quantities:

$$w = \frac{w^*}{h},\ r = \frac{r^*}{b},\ k = \frac{a}{b},\ t = \frac{t^*}{t_0},\ \Omega = \Omega^* t_0,\ \Delta p = \frac{\Delta p^* t_0^2}{r h^2} \qquad (1)$$

where t^* represents time and $t_0 = (12(1-n) r b^4 / (E h^2))^{1/2}$ is a characteristic time constant, the field equations become:

$$w_{,tt} + 2\Omega w_{,tj} + \Omega^2 w_{,jj} + D[w_{,t}] + K[w] = \Delta p + \frac{1}{r} f(t)\Big|_{\mathsf{A}} \tag{2}$$

$f(t)$ is the acoustic excitation and A is the surface of excitation. Further

$$K[w] = \nabla^4 w - \frac{1}{r}(rN_{rr} w_{,r})_{,r} - \frac{1}{r^2}(N_{jj} w_{,jj}) \tag{3}$$

is the self-adjoint stiffness operator modeling the bending stiffness and stiffeness caused by the membrane stresses (N_{rr}, N_{jj}) of rotation. Substrate material viscoelastic effects are introduced through the self-adjoint, positive definite operator $D[w_{,t}] = \nabla^4 w_{,t}$ where the material damping is assumed to be proportional to the rate of bending strain (Hosaka and Crandall (1992), Hansen *et al.* (1998)). Finally, the boundary and periodicity conditions for the plate deflection and aerodynamic pressure are given by

$$\begin{aligned}
&w\big|_{r=k} = 0, \quad (w_{,rr} + n(w_{,jj} + w_{,r}))\big|_{r=1} = 0, \\
&w_{,r}\big|_{r=k} = 0, \quad ((\nabla^2 w)_{,r} + (1-n)(w_{,r} - w)_{,jj})\big|_{r=1} = 0 \\
&w(r, j, t) = w(r, j + 2p, t) \\
&\Delta p(k, j, t) = 0, \quad \Delta p(1, j, t) = 0
\end{aligned} \tag{4}$$

Note that there are other boundary conditions governing the in-plane displacements of the disk, which are taken into account in calculating the membrane stresses due to rotation (D'Angelo and Mote (1993)).

2.1 Aeroelastic coupling

The Reynolds number of the flow in a hard disk drive is greater than that encountered in a floppy disk drive. Accordingly hydrodynamic lubrication theory, describing the pressure in a thin film between the disk and a rigid enclosure, is not applicable in this problem. At the same time, an analytical model of the pressure loading based on the complete Navier-Stokes equation is too complicated to be useful. For this reason we desire a simple model of aerodynamic loading that is based on a lubrication model.

A main feature of this lubrication model is that Δp can be described in terms of a distributed viscous damping that rotates at half the rotation speed of the disk (Hosaka and Crandall (1992)). The rotating damping speed being half of the disk rotation speed arises

because at very low Reynolds numbers, the mean flow speed in the gap is half of the disk speed. In our modeling, we retain the rotating damping model because it describes many of the experimental observation. However, no prescription of the speed of the rotating damping is provided. Instead, the speed will be deduced experimentally. Further, in the lubrication model, the speed of rotating damping is independent of the mode of vibration of the disk. We now allow the rotating damping speed to depend on the number of nodal diameters of the excited mode. This allows the following generalization of the aerodynamic loading (in ground-fixed frame):

$$\nabla^2(\Delta p) = -a\,(w_{,t} + (\Omega - \Omega_{dmn})w_{,j}) \tag{5}$$

where a is a positive parameter dependent on the viscosity of the fluid, the rotation speed Ω and the gap width. Further, (m,n) are the nodal circle and nodal diameter number of the particular mode of vibration. Thus, this generalization allows the rotating damping speed to depend on the excited mode, as well as allowing a nonlinear variation of the rotating damping speed with disk speed. Choosing the speed of rotating damping $\Omega_{dmn} = \Omega/2$ yields the lubrication theory model for pressure loading. Note also that we are neglecting the effects of radial flow (Huang and Mote (1996)) in this analysis because the radial flow effect in this shrouded disk is shown experimentally not to be significant. This is borne out by the experiments presented later in this work. Lastly, to address a question: are outer disks in a disk stack more susceptible to flutter? The speed of rotating damping with respect to the disk is expected to be greater in the gap between the disk and rigid enclosure than between two co-rotating disks since the mean flow in the disk-rigid enclosure gap is smaller because of high transverse shear. For this reason the highest probability for flutter occurs in a single disk with a base plate and a rigid cover on each side. Based on this reasoning we focus on a single disk in the disk stack. The following subsections on the coupled "eigenvalue problem" and "extraction of model parameters" are based on Hansen *et al.* (1998).

2.2 Coupled eigenvalue problem

Noting that the Laplacian is a self-adjoint operator and considering the boundary conditions on Δp, the assumed aerodynamic loading (5) can be inverted with the help of Green's functions (Renshaw (1998)), $\Delta p = -C[w_{,t}+(\Omega-\Omega_{dmn})w_{,j}]$ with C being a self-adjoint operator. Assuming a solution of the separable form:

$$w(r,j,t) = R_{mn}(r)e^{inj+lt} \tag{6}$$

where $R_{mn}(r)$ is in general a complex valued function and (m,n) are the number of nodal circles and diameters, respectively of the mode in question. Substituting this form into equation (2), in the absence of acoustic excitation yields the coupled aeroelastic eigenvalue problem:

$$(l^2+i2\,ln\Omega-n^2l^2)R_{mn}+K_n^r[R_{mn}]+lD_n^r[R_{mn}]+(l+in(\Omega-\Omega_{dmn}))C_n^r[R_{mn}] = 0 \tag{7}$$

where (K_n^r, D_n^r, C_n^r) are one dimensional differential operators obtained by the substitution of the assumed mode shape into the spatial operators (K, D, C). Aeroelastic coupling between modes possessing different number of nodal circles is neglected (Hansen *et al.* (1998)). Taking inner products of equation (7) with each eigenfunction gives

$$(l_{mn}+in\Omega)^2+w_{mn}^2+c_{mn}(l_{mn}+in(\Omega-\Omega'_{dmn})) = 0 \tag{8}$$

where $w_{mn}^2 = \langle R_{mn}, K_r^n[R_{mn}]\rangle$ are the uncoupled natural frequencies of the modes (co-rotating frame), and are given by (D'Angelo and Mote (1993))

$$w_{mn}^2 \approx (w_{mn}^{st})^2+s_{mn}\Omega^2 \tag{9}$$

where w_{mn}^{st} is the natural frequency of the same mode in a stationary disk. Further

$$c_{mn} = \langle R_{mn}, D_r^n[R_m]\rangle+\langle R_{mn}, C_r^n[R_m]\rangle \tag{10}$$

represents the combined effects of structural and co-rotating fluid damping, and

$$\Omega'_{dmn} = \Omega_{dmn}\frac{\langle R_m, C_r^n[R_m]\rangle}{c_{mn}} \tag{11}$$

where Ω'_{dmn} is the effective rotating damping speed modified by the ratio of aerodynamic co-rotating damping to the total co-rotating damping of the mode. Thus the greater the structural dissipation of the substrate material lower the effective rotating damping speed. Solution for the eigenvalues under assumption of weak damping yields:

$$l^F_{mn} = -\frac{c_{mn}}{2}\left(1+\frac{n\Omega'_{dmn}}{w_{mn}}\right)-i(w_{mn}+n\Omega), \quad l^B_{mn} = -\frac{c_{mn}}{2}\left(1-\frac{n\Omega'_{dmn}}{w_{mn}}\right)+i(w_{mn}-n\Omega) \qquad (12)$$

where the superscripts F and B refer to forward or backward traveling wave that propagate in the direction of disk rotation or against it, respectively. These waves are abbreviated FTW and BTW, respectively. Thus the immediate effect of the circulatory term in the aerodynamic pressure is to cause forward traveling waves to be more highly damped than the backward traveling waves. This phenomenon is seen in the hard disk drive at subcritical speeds; see Introduction. Further, the damping of a backward traveling wave in (12) can vanish at the onset of aeroelastic flutter. The condition for the onset of aeroelastic traveling wave flutter is:

$$\frac{w_{mn}}{n} = \Omega'_{dmn} \qquad (13)$$

or when the effective rotating damping speed equals an uncoupled wave speed on the disk. Similarly, from equation (12), we see that the frequencies of the backward and forward traveling waves split and at critical speed, $\Omega_c = \frac{w_{mn}}{n}$, the frequency of a BTW equals zero. Lastly, we note that the component of the FRF of the disk, acoustically excited at $(r_f^*, 0)$ and measured at (r_x^*, j_x), corresponding to the eigenvalue problem (8) is (Lee and Kim (1995))

$$H(w) \approx R_{mn}(r_f^*)R_{mn}(r_x^*)\left(H_{mn}e^{inj_x} + \overline{H}_{mn}(-w)e^{-inj_x}\right) \qquad (14)$$

where $H_{mn}(w) = \dfrac{1}{w_{mn}^2 - (w+n\Omega)^2 + ic_{mn}(w+n\Omega-n\Omega'_{dmn})}$. A detailed derivation of equation (14) is presented in Hansen *et al*. (1998).

2.3 Extraction of model parameters

From equations (9) and (12) we see that the model parameters that need to be identified from the experiment are $(s_{mn}, c_{mn}, \Omega'_{dmn})$ for each mode at each disk rotation speed. These parameters represent, respectively, the stiffeness coefficient due to rotation for the modal natural frequency, the total co-rotating modal damping, and the effective rotating damping

speed in that mode. These parameters can be obtained from the Frequency Response Function. Once the wave poles, $(a^F_{mn}+iw^F_{mn}, a^B_{mn}+iw^B_{mn})$, corresponding to forward and backward traveling waves are identified in the FRF, equations (9) and (12) give

$$
\begin{aligned}
s_{mn} &= \frac{\left(w^F_{mn} + w^B_{mn}/2\right)^2 - (w^{st}_{mn})^2}{\Omega^2} \\
c_{mn} &= a^F_{mn} + a^B_{mn} \\
c_{mn}\Omega'_{dmn} &= \frac{w_{mn}}{n}(a^F_{mn} - a^B_{mn})
\end{aligned}
\qquad (15)
$$

The experimentally obtained damping factors of the wave poles in the FRF, (a^F_{mn}, a^B_{mn}) are usually small, and to avoid errors in calculating Ω'_{dmn} through division by c_{mn}, we will calculate directly c_{mn} and the product $c_{mn}\Omega'_{dmn}$ through the above relations.

3 Experimental analysis

Experiments were performed to estimate the flutter speed of 3.5 inch hard disk drive. The flutter speed was estimated from the condition (13) through the extrapolation of the effective rotating damping speeds and wave speeds. The effects of the air gap, the distance between the disk surface and cover, on the critical speeds and flutter speeds was also investigated by performing the test with cover positioned at different gaps.

3.1 Experimental setup

The out of plane vibration of the disk was measured using a Laser Doppler Displacement Meter (LDDM) through a hole (1 mm in diameter) in the cover as shown in Fig. 2.. A speaker (0.1 Watt, 8 Ohms, 2 inch in diameter) was used to excite the disk through a hole (20 mm in diameter) in the cover. The current to the speaker gave a measure of the input to frequency response function and the signal from the disk vibration was the output. A white noise excitation signal was input to the speaker and FRF was measured at the disk speeds from 6,000 rpm to 19,800 rpm.

"Labview" was used to collect the data and calculate FRF from the input / output signals. The damping factors of each mode were calculated by curve fits in Matlab to the measured FRF.

3.2 Estimation of wave frequencies and damping factors

In this experiment, the frequency resolution was 0.183 Hz (6 kHz cut-off frequency and 65,536 frame size) and the 3 dB bandwidth of the resonance peaks was in the range of 0.5-5 Hz. With this frequency resolution, sufficient data were recorded for both forward and backward resonance peaks to estimate the damping factors.

The FRF was processed on PC to obtain the wave frequencies and damping factors of four modes (m = 0 and n = 2,3,4,5). Because the (0,1) mode has no critical speed, i.e. $w_{01} > \Omega, \forall \Omega$ (Renshaw & Mote, 1992), and assuming $\Omega_{d01} < \Omega$, it is expected that no flutter can occur in this mode. For this reason, the (0,1) mode was not measured. To improve the estimation of modal parameters, a large number of average was required (approximately 100). Because of large frame size in FRF, the higher frequency resolution required extended recording time to collect the data with sufficient averaging. Fluctuation of the disk speed was found during the extended recording time. This rotation speed fluctuation can cause error in calculating the modal parameters. For example, a 0.5 Hz fluctuation in rotation speed during the measurement will cause approximately ± 0.5×n Hz difference in the forward and backward wave frequency peak for (0,n) mode. This speed fluctuation causes significant error in evaluating the damping factor. Because the typical 3 dB bandwidth of the backward resonance peaks in this experiment is in the range of 0.5-2 Hz, an error in of ± 2.5 Hz (say, for (0,5) mode) by speed fluctuation causes the evaluated damping factors to be much larger than the correct value. For this reason, a frequency response spectrum averaged over 100 ensembles causes significant error in the damping measurement. To minimize the error in the damping factors with speed fluctuation, the FRF was averaged after only 3 ensembles and the speed fluctuation was monitored through the runout frequency of the disk vibration. For each such data set, the speed was constant. 33 such averaged data sets were collected (each from 3 averaged ensembles). The speed may vary from one data set to another. These speed fluctuations, Δf, were used to correct the resonance peaks for different data sets by shifting frequencies by ± n ×Δf Hz. The

peaks in each data set were adjusted to coincide and an averaged FRF over data 33 sets was calculated and used obtain the wave frequencies and damping factors.

The peaks from each wave frequencies are assumed to describe the single degree of freedom oscillator. Curve fitting was performed on the amplitude of FRF near each peak to obtain modal parameters. The wave frequencies and damping factors are calculated with different bandwidth taken near the peak in curve fitting. Curve fits are performed for 12 different bandwidth for the same peak. The modal parameters from the bandwidth that result in the largest correlation coefficient during curve fitting were chosen as the values of the wave frequency and damping factor.

Forward and backward wave frequencies were measured at disk speeds from 6,000 rpm to 19,800 rpm. This experiment was repeated with changing air gaps between the disk and the cover, *d*. The natural frequencies at each speed from forward and backward wave frequencies are obtained using the relationships $w_{0n}^{F} \approx w_{0n} + n\Omega$, $w_{0n}^{B} \approx w_{0n} - n\Omega$ and are curve fitted by equation (9), $w_{0n}^{2} = w_{0n}^{st\ 2} + s_{0n}\Omega^{2}$. The results of the curve fits are shown in Table 1. The correlation coefficients R^2 in Table 1 shows that (9) is a reasonable approximation of the relationship between the disk speed and the natural frequency for all the tests. Wave frequencies from experiments are shown in Fig. 3. Also shown in Fig. 3 are the wave frequencies after curve fitting based on the relationship (9).

Estimated critical speeds with changing air gap are shown in Fig. 4. It is observed that the critical speeds of the four modes is higher when the disk is uncovered. The percentage increases in critical speeds of uncovered case, compared to the averaged critical speeds in covered cases, are 4.1, 3.4, 3.9, 4.5 % for 2, 3, 4, 5 modes respectively.

The estimated damping factors of the forward/backward travelling waves for the 4 modes at different gap width, as function of disk speed, are shown in Fig. 5. It is observed that the damping factors of FTWs are substantially larger than those of the BTWs. The differences increase with increasing disk speed. We also see Fig. 6 that the absolute values of damping factors of FTWs and BTWs tend to decrease with increasing air gap.

3.3 Estimation of aeroelastic parameters and flutter speeds in disk drive

After the damping factors a_{0n}^{F} and a_{0n}^{B} are obtained, the two aeroelastic parameters c_{0n} and $c_{0n}\Omega'_{d0n}$ can be extracted as shown in equation (15),

$$c_{0n} \approx a_{0n}^{F} + a_{0n}^{B} \ , \quad c_{0n}\Omega'_{d0n} \approx w_{0n}\frac{(a_{0n}^{F} - a_{0n}^{B})}{n} .$$

The damping coefficients c_{0n} tend to increase linearly with disk speed, whereas the product $c_{0n}\Omega'_{d0n}$ tends to increase nonlinearly with disk speed. Linear and second order polynomial functions of disk speed were chosen to curve fit the two aeroelastic parameters c_{0n} and $c_{0n}\Omega'_{d0n}$ respectively.

$$c_{0n} \approx c_1 + c_2\Omega \ , \quad c_{0n}\Omega'_{d0n} \approx c_3\Omega + c_4\Omega^2 \tag{16}$$

Typical values of c_{0n} and $c_{0n}\Omega'_{d0n}$ of the four modes with increasing disk speed and their curve fits based on (16) are shown in Fig. 7 (d = 0.15 inch). The four fitting coefficients c_1, c_2, c_3, c_4 and the correlation coefficients R^2 for the four modes are shown in Table 2.

With these expressions for c_{0n} and $c_{0n}\Omega'_{d0n}$ the effective damping speed Ω'_{d0n} can be estimated as

$$\Omega'_{d0n} \approx \frac{c_3\Omega + c_4\Omega^2}{c_1 + c_2\Omega} \tag{17}$$

By extrapolating the curves for the effective damping speeds, the flutter speed of each case tested here can be estimated by the intersection of the wave speed curve w_{0n}/n and the effective damping speed curve Ω'_{d0n} of each mode. The effective damping speeds estimated in this manner together with wave speeds for each mode and air gap are shown in Fig. 8.

The trend of effective damping speed in each mode with varying air gap can be observed in this plot. For example, in the (0,4) mode there exists no flutter speed when the air gap is 0.05 inch. As the air gap increases, the effective damping speed intersects the wave speed curve when the air gap lies between 0.1 and 0.15 inch. As the air gap increases further, the slope of the effective damping speed curve decreases and intersection with the wave speed vanishes for $0.35 < d < \infty$. Even though this behavior in other modes is not as clear as in (0,4) mode in Fig. 8, the general trend can be seen in Fig. 9. In (0,2)

and (0,3) modes, the flutter speeds decrease with increasing air gap, whereas in (0,5) mode the flutter speed increases with increasing air gap. The flutter speeds in each mode and at each air gap are listed in Table 3.

Aeroelastic flutter is predicted to occur in the (0,3) mode at each air gap except d = 0.15 inch. The smallest flutter speed was predicted to be 34,970 rpm (d = 0.35 inch, (0,3) mode).

4 Discussion

Natural frequencies and critical speeds of the (0,2) (0,3), (0,4), (0,5) modes were found to be consistently greater for an uncovered disk; see Fig. 2 and Fig. 3. Removal of the cover decreases the bending stiffness of the spindle. Because only the (0,1) mode on the disk is coupled to spindle bending (Parker and Mote (1996)) it is expected that removal of the cover decreases the frequency of the (0,1) mode while maintaining unchanged the frequencies of the higher modes. For this reason the observed increases in frequencies of the higher modes for the uncovered disk were unexpected. One possible reason for this phenomenon is based on the presence of thermal gradients on the rotating disk. Due to friction, heat is generated in the bearings which is transferred through the collars to the disk. The resulting temperature gradients modify the membrane stresses and thus the frequencies of the rotating disk. Owing to flow re-circulation in a covered disk, the temperature of the airflow is significantly greater than in an uncovered case. Consequently the radial temperature gradient of the uncovered disk is expected to be larger than in the covered disk. This can result in higher natural frequencies in the uncovered case compared to the covered case. This agrees with the results of Nieh and Mote(1972) who found the increased critical speeds (in (0,2) and (0,4) modes, numerically and experimentally) when bearing heating was applied at the inner radius of the rotating disk.

Decreasing air gap between the disk and the cover leads to increased damping factors (see Fig. 6). Recently, Ono *et al*. (1999) studied the effect of partial squeeze air bearing plate, which is located on top of the disk, on the amplitude of disk vibration. They found that the amplitude of travelling wave of the lowest frequency decreases with decreasing the

air gap between the disk surface and the air bearing plate at 7,200 and 9,600 rpm. The present work supports and explains their observation.

Increased material damping in the disk substrate suppresses the onset of flutter. Increased modal damping of the substrate, $\langle W_{0n}, D[W_{0n}]\rangle$, results in decreased effective damping speed (equations (10), (11)), and consequently greater aeroelastic flutter speed. For a disk of given clamping ratio and bending stiffness, it may be possible to choose a substrate material with sufficient internal damping to eliminate aeroelastic instability.

Damping factors predicted from hydrodynamic lubrication theory correlate poorly with experimental results. A lower bound for the speed of aeroelastic flutter in this case is provided by the condition that that the rotating damping speed $\Omega_d = \Omega/2$ equals the undamped wave speed w_{0n}/n as the disk speed is increased. Inclusion of material damping through effective rotating damping speed will increase this estimate. However, it is found in the experiments that there is no intersection of the rotating damping and wave curves as speed changed. This implies that use of hydrodynamic lubrication theory will never predict flutter of the disk at any speed. Hydrodynamic lubrication theory for Δp (Hosaka and Crandall (1992), Renshaw (1998), Pelech and Shapiro (1964)) prescribes that c_{0n} and $c_{0n}\Omega'_{d\,0n}$ should be respectively, constant and a linear function of the disk speed.

$$c_{0n} \approx c_5 \ , \quad c_{0n}\Omega'_{d\,0n} \approx c_6\Omega \tag{18}$$

R^2 for c_{0n} is zero by the definition of correlation coefficient. The correlation coefficients for $c_{0n}\Omega'_{d\,0n}$ based on the curve fits (16) and (18) are shown in Fig. 10. It can be seen that the R^2 values from curve fit (16) lie within 0.9 ~ 1 whereas those from curve fit (18) lie in the range 0.75 ~ 0.85. From this, it can be said that hydrodynamic lubrication models of the airflow between a disk and cover predict poorly the differential damping of forward and backward traveling waves observed in the experiment.

The experiments indicate that the radial flow in the air gap does not significantly effect aeroelastic flutter of the covered disk. Huang and Mote (1995) note that secondary radial flow introduces a non-symmetric film stiffness acting on the spinning disk. This effect introduces an instability in addition to the rotating damping instability described in this

work. Huang and Mote (1995) show that at pre-flutter speeds, the effect of the film stiffness is to split the wave speeds of a given mode. In the present work, wave speeds calculated for a particular mode from forward and backward traveling frequencies in the experiment, were found to be less than 2.5% apart from each other. This indicates the effects of radial flow are not significant in the present disk drive. One reason for this could be that because of the radial shroud, the radial flow velocities are lower in a disk drive than in an open disk case considered by Huang and Mote (1995).

Lastly, owing to the high Reynolds number in the gap of an actual disk drive the resulting flow is usually unsteady. Unsteadiness of the pressure fluctuations cause wide band excitation of the disk at all rotation speeds. The aeroelastic instability referred to in this work arises due to bulk or average motion of the fluid in the gap with respect to the disk and cannot predict the effects of turbulent pressure fluctuations on disk vibration at pre-flutter speeds. For this reason, aeroelastic traveling wave flutter can be regarded as an upper bound for operation speeds in disk drives. Turbulence induced vibration of disks can prevent operation of disk drives even at pre-flutter speeds.

5 Conclusions

An experimental technique is presented to estimate the flutter speed of a hard disk drive. Model parameters are extracted from the FRF of an acoustically excited disk spinning at sub-critical speeds ranging from 6,000-19,800 rpm. The flutter speed was estimated through the extrapolation of the effective rotating damping speeds and wave speeds. The results indicate that aeroelastic flutter speeds can be as low as 35,000 rpm and depend significantly on the air gap between the disk and the cover. Aeroelastic flutter is not predicted to occur near 20,000 rpm for the impending generation of disk drives. However, if the substrate material remains unchanged, it is expected to be a problem for 30,000+ rpm drives. The technique presented in this work can also be extended to estimate the flutter speeds in optical disks including DVD and CDROM drives,which are already operating at supercritical speeds and closer to their limits of aeroelastic instability. Experimental estimation of flutter speeds in these devices will be important for the design of the impending generation of optical drive.

References

Chonan S, Jiang ZW and Shyu YJ, 1992, “Stability analysis of a 2" floppy disk drive system and the optimum design, of the disk stabilizer”, *Journal of Vibration and Acoustics*, Vol. 114(2) 283-286.

D’Angelo, C. and Mote, C.D., Jr., 1993, “Natural frequencies of a thin disk, clamped by thick collars with friction at the contacting surfaces, spinning at high rotation speed”, *Journal of Sound and Vibration*, Vol. 168(1), 1-14.

Hansen, M.H., Raman, A and Mote, C.D., Jr., 1999, “Estimation of non-conservative aerodynamic pressure leading to flutter of spinning disks”, Technical report No. 605, *Danish center for applied mathematics and mechanics, Technical University of Denmark*.

Hosaka, H. and Crandall, S., 1992, “Self-excited vibrations of a flexible disk rotating on an air film above a flat surface”, *Acta Mechanica*, Vol. 3,115-127.

Huang, F. and Mote, C.D., Jr.,1995, “On the instability mechanism of a disk rotating close to a rigid surface”, *Journal of Applied Mechanics*, Vol. 62,764-771.

Huang, F. and Mote, C.D., Jr.,1996, “Mathematical analysis of stability of a spinning disk under rotating, arbitrarily large damping forces”, *Journal of Vibration and Acoustics*, Vol. 118(4), 657-662.

Lee, C.-W. and Kim, M.-E.,1995, “Separation and identification of travelling wave modes in rotating disk via directional spectral analysis”, *Journal of Sound and Vibration*, Vol. 187(5), 851-864.

Lee, S. Y. and Kim. S. K., 1998, “Trends and mechanical issues in optical disk drives”, *Proceedings of the 9th International Symposium on Information Storage and Processing Systems*, Vol. 4, 81-90.

Nieh, L. 1972, “Rotating disk stability ; Spectral analysis and thermal effects”, *Ph. D. thesis, University of California at Berkeley*.

Parker, R. and Mote, C.D., Jr., 1996, “Vibration and coupling phenomena in asymmetric disk-spindle systems”, *Journal of Applied Mechanics*, Vol. 63,(4) 953-961.

Pelech, I. And Shapiro, A. H., 1964, “Flexible disk rotating on a gas film next to a wall”, *Journal of Applied Mechanics*, Vol. 31, 577-584.

Renshaw, A., 1998, “Critical speeds for floppy disks”, *Journal of Applied Mechanics*, Vol. 65(1), 116-120.

Renshaw, A. and Mote, C.D., Jr., 1992, “Absence of one nodal diameter critical speed modes in an axisymmetric rotating disk”, *Journal of Applied Mechanics*, Vol. 59, 687-688.

	d (inch)	(0.2)B	(0,2)F	(0,3)B	(0,3)F	(0,4)B	(0,4)F	(0,5)B	(0,5)F
w_{0n}^{st}	0.05	719.58	708.47	1161.4	1154.3	1911.9	1904.0	2899.5	2891.4
	0.1	722.16	711.23	1164.4	1158.4	1916.1	1909.3	2904.9	2897.7
	0.15	721.21	712.13	1164.7	1160.3	1916.3	1911.1	2904.7	2899.6
	0.25	723.23	713.91	1166.1	1161.7	1917.7	1912.6	2906.5	2900.7
	0.35	724.70	715.01	1167.0	1162.8	1919.0	1914.2	2908.3	2903.2
	Open	724.38	715.47	1166.4	1162.7	1918.2	1913.9	2907.7	2903.0
s_{0n}	0.05	1.5434	1.4751	1.9984	1.8822	2.4164	2.2718	2.7831	2.5803
	0.1	1.5416	1.5001	1.9844	1.9053	2.4029	2.2997	2.7775	2.6345
	0.15	1.5525	1.5096	1.9955	1.9174	2.4205	2.3191	2.8070	2.6596
	0.25	1.5428	1.5083	1.9846	1.9151	2.4070	2.3143	2.7826	2.6565
	0.35	1.5399	1.5066	1.9852	1.9187	2.4103	2.3198	2.7975	2.6678
	Open	1.5810	1.5470	2.0670	2.0020	2.5565	2.4657	3.0314	2.9045
R^2	0.05	0.99996	0.99998	0.99995	0.99997	0.99998	0.99998	0.99998	0.99998
	0.1	0.99998	0.99999	0.99998	0.99998	0.99998	0.99999	0.99999	0.99999
	0.15	0.99986	0.99999	0.99998	0.99999	0.99999	0.99999	0.99999	0.99999
	0.25	0.99998	0.99999	0.99997	0.99999	0.99998	0.99999	0.99999	0.99999
	0.35	0.99997	0.99999	0.99997	0.99998	0.99998	0.99999	0.99999	0.99999
	Open	0.99998	0.99999	0.99998	0.99999	0.99999	0.99999	0.99999	0.99999

Table 4.1 Natural frequencies w_{0n}^{st}, centrifugal stiffening coefficients s_{0n} and correlation coefficients of curve fits.

mode	d (inch)	c_1	$c_2 \times 100$	$R^2(c_{0n})$	c_3	$c_4 \times 100$	$R^2(c_{0n}\Omega'_{d0n})$
(0,2)	0.05	2.9522	1.3799	0.97695	1.0893	1.0676	0.95266
	0.1	1.0753	1.4102	0.98259	-0.1260	1.2273	0.98578
	0.15	1.7703	0.8978	0.98582	-1.0339	1.3136	0.98184
	0.25	1.7014	0.7632	0.89043	-0.5847	1.0146	0.97915
	0.35	1.4710	0.7498	0.96845	-0.1855	0.79367	0.96430
	Open	1.1776	0.4731	0.92048	-0.3222	0.63575	0.95530
(0,3)	0.05	1.1601	1.6783	0.99000	1.26250	1.17030	0.96069
	0.1	1.3046	0.8527	0.93587	0.40608	0.84232	0.94322
	0.15	0.9622	0.8110	0.96367	0.27104	0.73037	0.95423
	0.25	1.1576	0.6635	0.93922	0.00745	0.73655	0.96577
	0.35	0.9253	0.6602	0.97175	-0.4134	0.83367	0.97644
	Open	0.7348	0.4969	0.95462	-0.1303	0.60916	0.96551
(0,4)	0.05	1.4375	1.0963	0.96456	3.4340	0.14476	0.93886
	0.1	0.4031	1.0163	0.93717	0.89724	0.44442	0.92928
	0.15	0.3813	0.8705	0.98368	0.29137	0.64845	0.96922
	0.25	0.3729	0.8034	0.94507	-0.1344	0.70821	0.96945
	0.35	0.3272	0.6872	0.98362	0.20321	0.50276	0.98952
	Open	0.4050	0.5183	0.96570	0.35333	0.31367	0.91999
(0,5)	0.05	1.3301	0.9142	0.89593	1.16730	0.78628	0.91255
	0.1	0.3695	0.8762	0.92372	0.08672	0.74092	0.94534
	0.15	0.6704	0.6003	0.98087	0.04142	0.63089	0.99232
	0.25	0.5874	0.6482	0.94424	0.25690	0.52775	0.94665
	0.35	0.4117	0.5111	0.97414	0.50409	0.29189	0.89809
	Open	0.5737	0.3843	0.95549	0.65017	0.08712	0.89376

Table 4.2 Curve fit coefficients to c_{0n} and $c_{0n}\Omega'_{d0n}$ and their correlation coefficients.

d (inch)	(0,2) mode	(0,3) mode	(0,4) mode	(0,5) mode
0.05	none	74,418	none	51,451
0.1	74,592	40,738	none	56,600
0.15	36,693	46,931	63,420	46,567
0.25	39,780	39,404	50,853	61,770
0.35	41,585	34,970	67,950	none
Open	43,195	35,420	none	none

Table 4.3 Flutter speeds (rpm) in the four modes under the change of air gap.

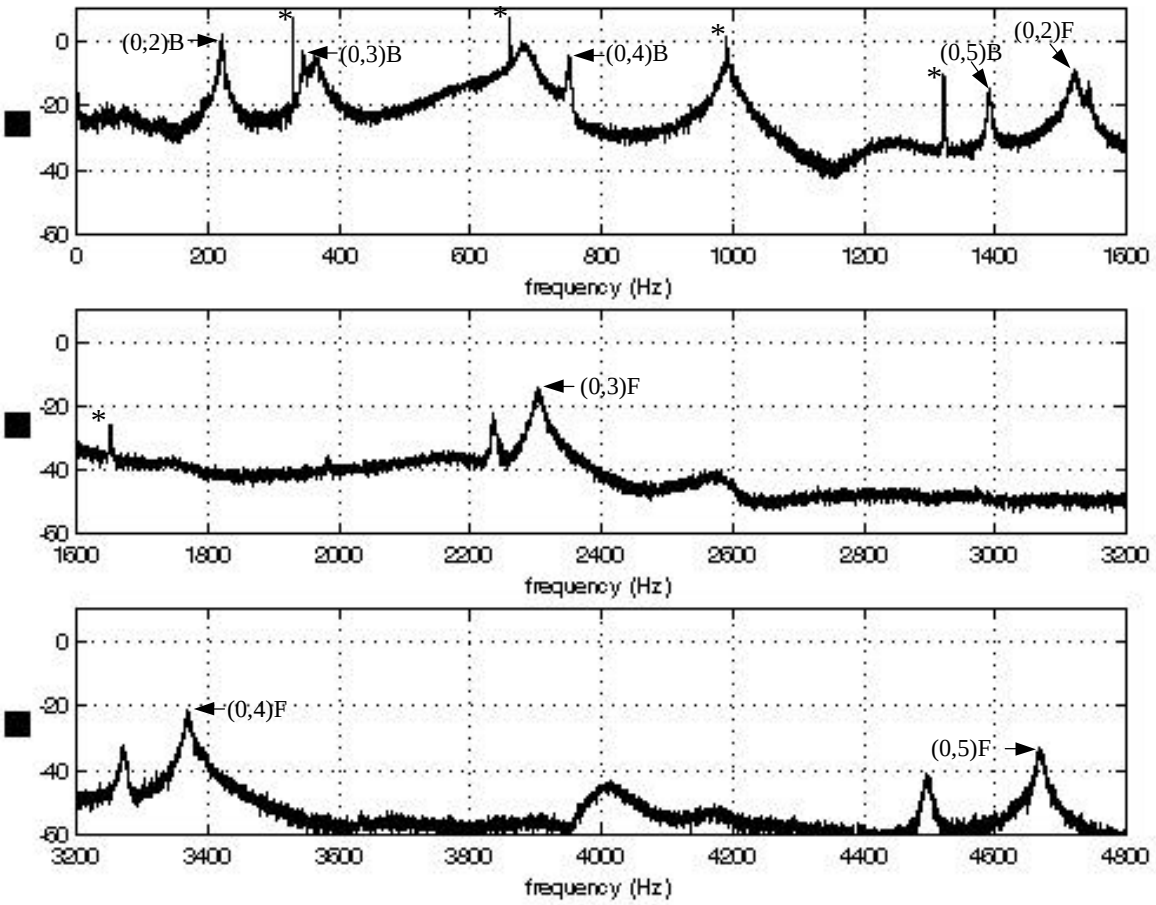

Fig. 1 Magnitude of frequency response function of aerodynamically exited disk.
(Disk speed : 19,800 rpm, ✳ : runout frequencies)
(m,n) refers to number of nodal circles and diameters, respectively of the travelling wave.
B and F represent backward and forward travelling waves.

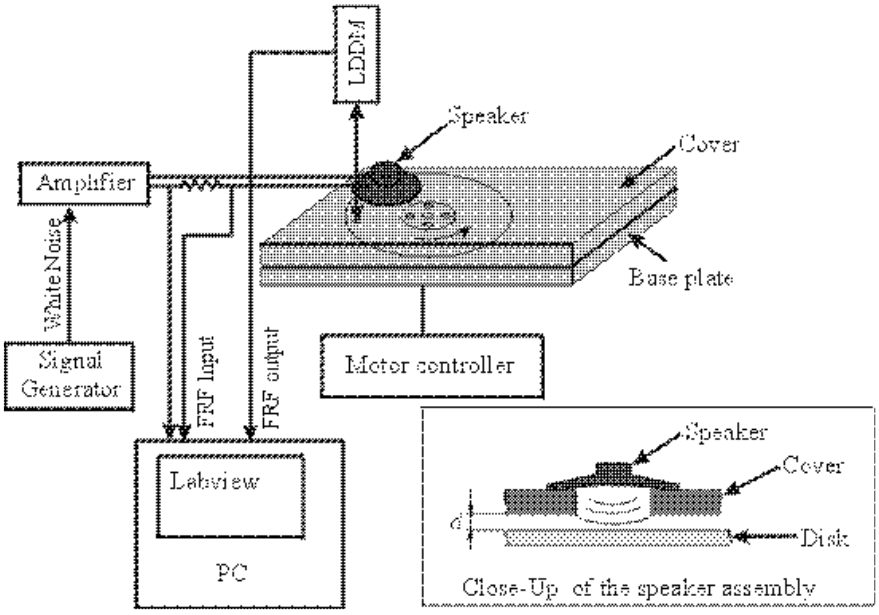

Fig. 2 Experimental Setup for measuring FRF of disk.

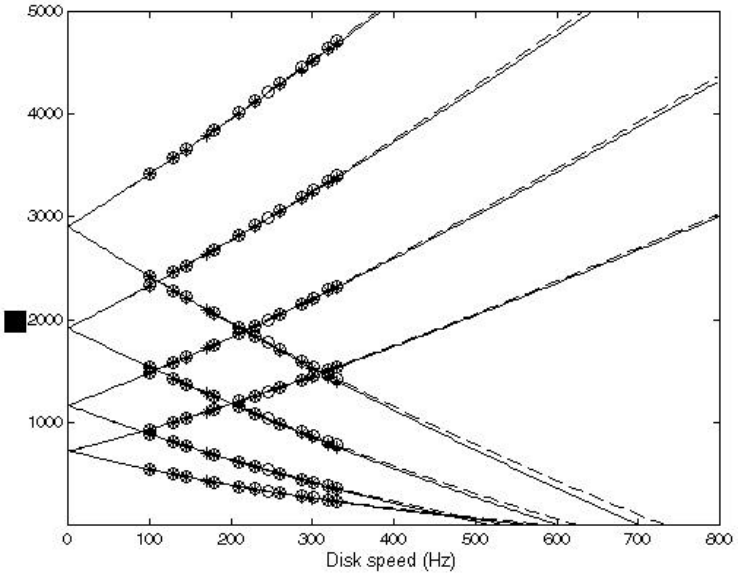

Fig. 3. Wave frequencies

✳ , — : from measurement and curve fit on w_{0n} , covered (d = 0.35 inch),

, -- - : from measurement and curve fit on w_{0n} , uncovered

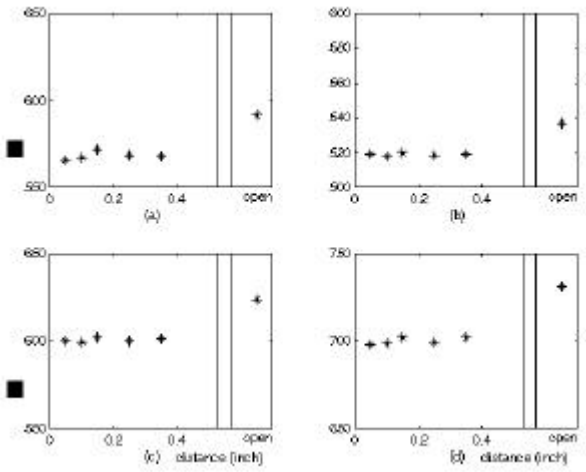

Fig. 4 Critical speed vs. air gap *d*.
(a) : (0,2) mode, (b) : (0,3) mode, (c) : (0,4) mode, (d) : (0,5) mode

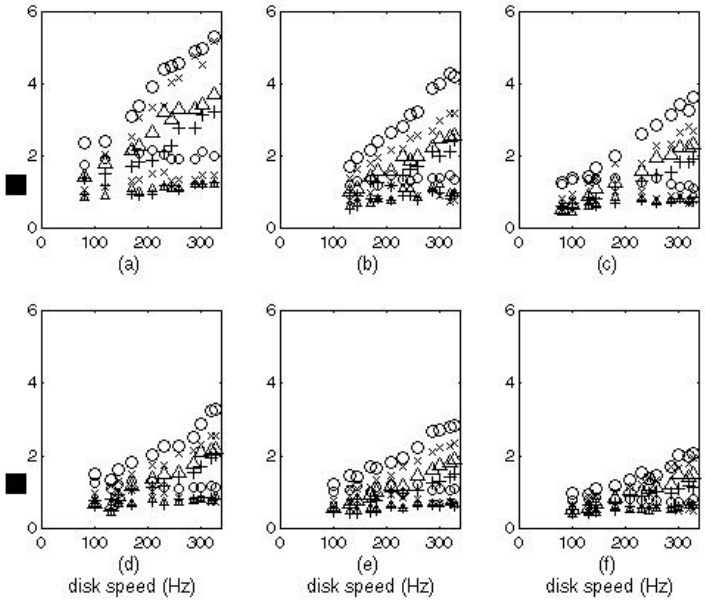

Fig. 5 Damping factors vs. disk speed.
(a): d = 0.05, (b) : d = 0.1, (c) : d = 0.15, (d) : d = 0.25, (e) : d = 0.35 inch,
(f) : uncovered
: (0,2) mode , × : (0,3) mode, : (0,4) mode, + : (0,5) mode
(Large marker: FTW, Small marker : BTW)

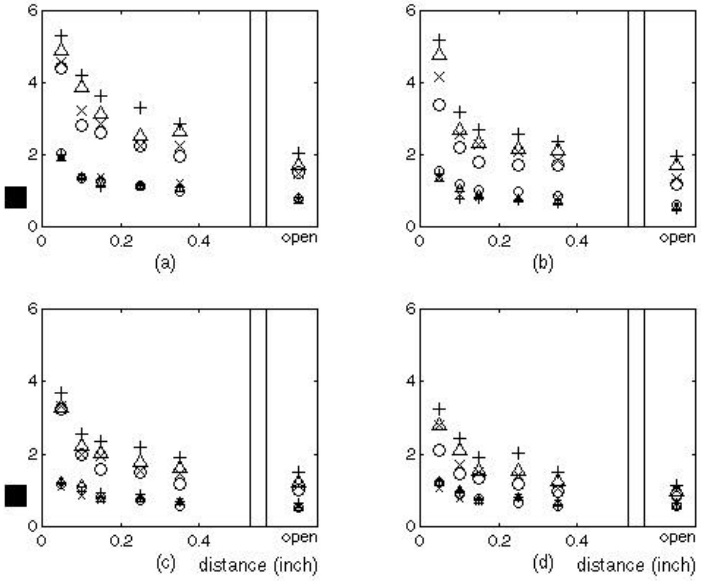

Fig. 6 Damping factors vs. air gap *d*.
(a) : (0,2) mode, (b) : (0,3) mode, (c) : (0,4) mode, (d) : (0,5) mode
: 13,800 rpm , × : 15,600 rpm, : 17,400 rpm, + : 19,800 rpm
(Large marker: FTW, Small marker : BTW)

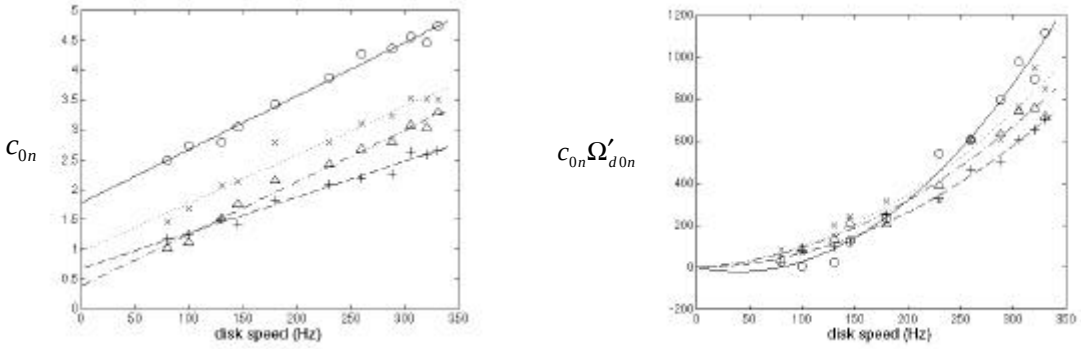

Fig. 7 Aeroelastic parameters c_{0n} and $c_{0n}\Omega'_{d0n}$ and their curve fits.
: (0,2) mode , × : (0,3) mode, : (0,4) mode, + : (0,5) mode

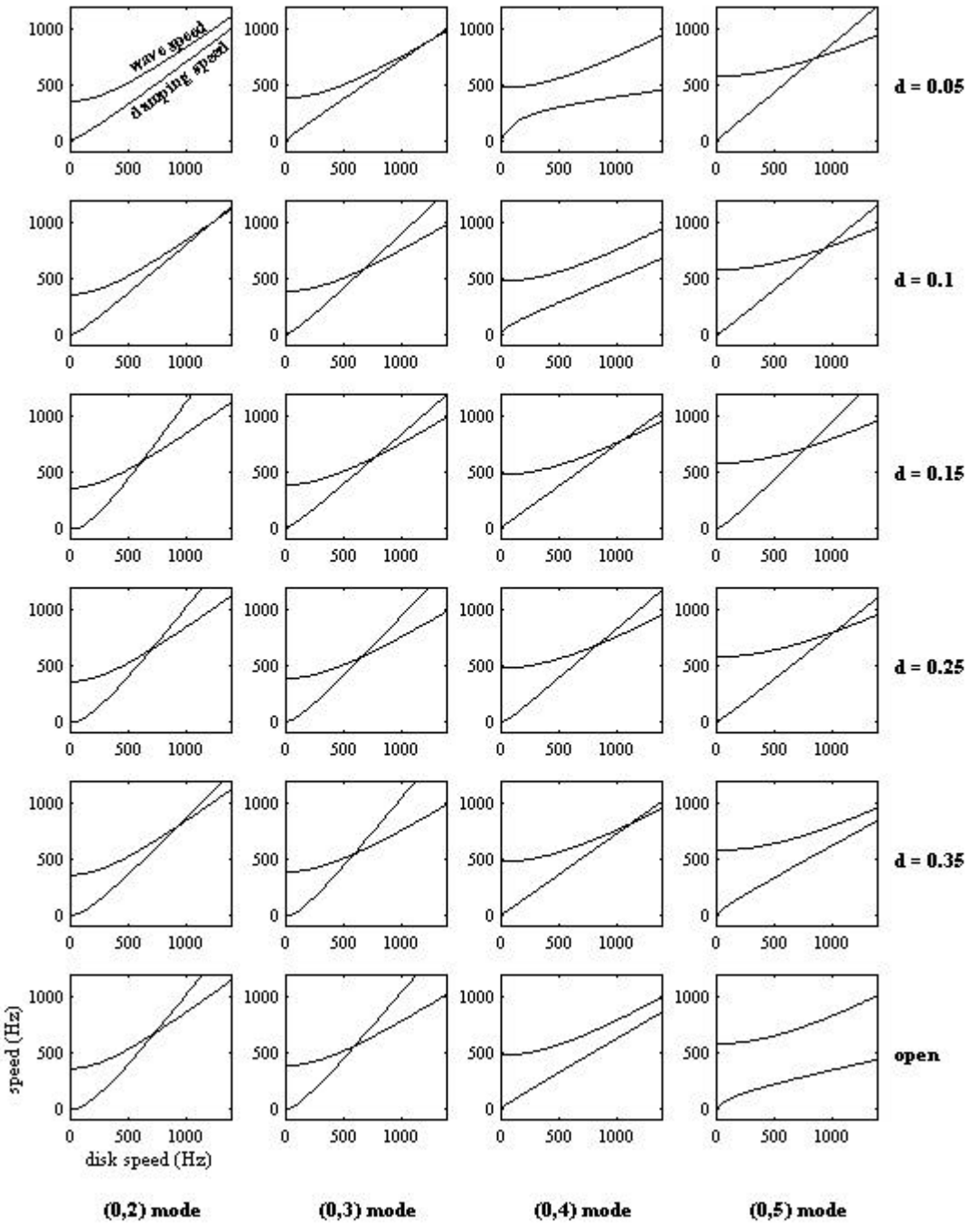

Fig. 8 Wave speeds $\frac{w_{0n}}{n}$ and damping speeds Ω'_{d0n} for each node under air gap change.

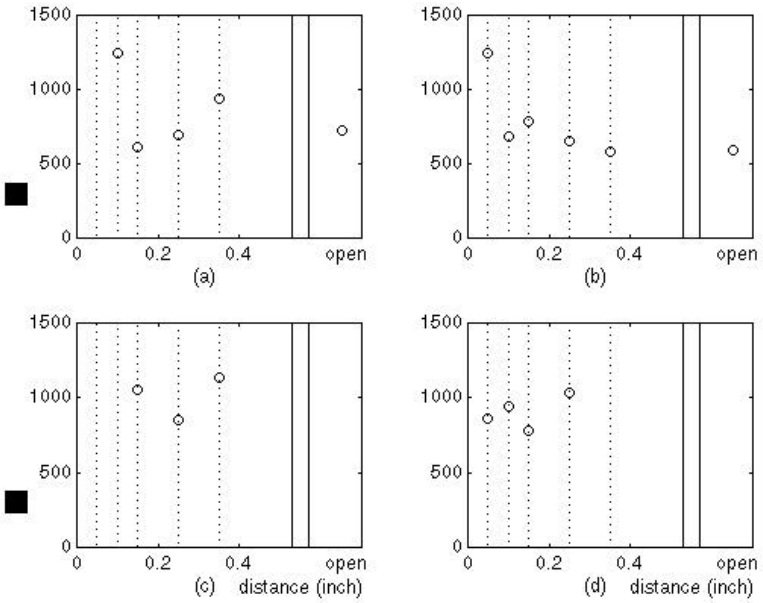

Fig. 9 Flutter speed of each mode vs. air gap.
(a) : (0,2) mode, (b) : (0,3) mode, (c) : (0,4) mode, (d) : (0,5) mode

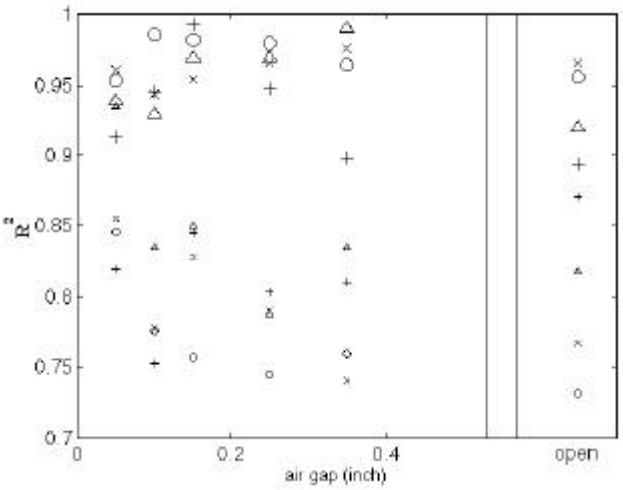

Fig. 10 Correlation coefficients for $c_{0n}\Omega'_{d\,0n}$ based on the curve fits.
: (0,2) mode , × : (0,3) mode, : (0,4) mode, + : (0,5) mode
Large markers : curve fit based on this work (equation (4.16))
Small markers : curve fit based on lubrication theory (equation (4.18))